PCCP

Accepted Manuscript

ROYAL SOCIETY OF CHEMISTRY

www.rsc.org/pccp

Journal Name

ARTICLE

The new insight into the structure-activity relation of Pd/CeO_2-ZrO_2-Nd_2O_3 catalysts by Raman, in situ DRIFTS and XRD Rietveld analysis

Received 00th January 20xx,
Accepted 00th January 20xx

DOI: 10.1039/x0xx00000x

www.rsc.org/

X. Yang, L. Yang, J. Lin, R. Zhou*[a]

Pd/CeO_2-ZrO_2-Nd_2O_3 (CZN) catalysts with different CeO_2/ZrO_2 molar ratios were synthesized and have been characterized by multiple techniques, e.g. XRD in combination with Rietveld refinement, UV-Raman, XPS and in situ DRIFTS. The XRD pattern of CZN with CeO_2/ZrO_2 molar ratios ≥ 1/2 can be indexed satisfactorily to the fluorite structure with a space group Fm-3m, while the XRD patterns of CZ12 only display diffraction peaks of tetragonal phase (S.G. P42/nmc). Nd addition can effectively stabilize the cubic structure of CZN support and increase the enrichment of defect sites on the surface, which may be related to the better catalytic activity of Pd/CZN12 catalysts compared with Pd/CZ12. The presence of moderate ZrO_2 can increase the concentration of O* active species, leading to accelerate the formation of nitrate species and thus enhance the catalytic activity of NO_x and HC elimination. The Pd-dispersion decreases with the increasing Zr content, leading to the decreased CO catalytic activity, especially for the aged catalysts. The change regularity of OSC value is almost the same with the in situ dynamic operational window, demonstrating that the in situ dynamic operational window is basically affected by OSC value.

1. INTRODUCTION

It is now well acknowledged that ceria promotes the performance of Three-way catalysts (TWCs) for the removal of pollutant gaseous products from automobile exhaust fumes. Ceria improves noble metal dispersion and stabilization as well as stores and releases oxygen.[1-5] However, a major drawback of ceria is the severe deactivation during high temperature process due to the sintering of ceria. Ceria-zirconia mixed oxides have gradually replaced pure ceria as oxygen storage materials since 1993, because the incorporation of Zr favours the formation of structural defects, accelerates the diffusion of bulk oxygen, enhances the thermal stability of supports and improves the catalytic activity at metal–support interfacial sites.[2-10]

As emission regulations are continuously being tightened, the new-generation three-way catalyst requires better thermal stability and higher OSC of oxygen storage component. A great deal of research efforts has shown that the addition of transition metals or rare earth metals (La, Pr and Nd) is beneficial to improve the thermal stability and to increase the OSC of ceria-zirconia solid solution by increasing the oxygen vacancies in the fluorite lattice.[11-15] Moreover, rare earth elements are often used considering their better thermal stability compared with transition metals. In our previous work, we found that the addition of neodymia would lead to the formation of homogenous CeO_2-ZrO_2-Nd_2O_3 (CZN) ternary solid solution with enhanced textural/structural properties as well as the higher OSC and improved redox behaviour, resulting in the promoted three way catalytic activity and enlarged air/fuel operational window. The modified solid solution with 5 wt.% neodymia showed the relatively better textural and structural properties considering that the capacity of foreign cation is limited in the crystal lattice of ceria–zirconia solid solution.[16]

Nevertheless, there is not a general agreement about the composition ratio for the ternary structure. The host/guest cation should preferably induce stress and structural defects due to the difference in the ionic radius between cations.[17] In the mixed oxides, the CeO_2/ZrO_2 molar ratio strongly affects the structure/texture properties of CeO_2-ZrO_2 mixed oxides, such as crystal structure, thermal stability, redox properties and the oxygen storage/release capacity (OSC).[18-20] However, the studies on the doping Nd_2O_3 effect on CeO_2-ZrO_2-based mixed oxides with different CeO_2/ZrO_2 molar ratios as important materials for TWC have rarely documented.

On the basis of that, we synthesized a series of CeO_2-ZrO_2-Nd_2O_3 mixed oxides with different CeO_2/ZrO_2 molar ratios to obtain the doping effect of Nd_2O_3 on structure-activity relation in CeO_2-ZrO_2, as well as the application in corresponding Pd-only catalysts for automobile emission control. Their structures were characterized by the Rietveld

[a] Institute of Catalysis, Zhejiang University, Hangzhou 310028, P. R China.
†Electronic Supplementary Information (ESI) available: The selectivity of N_2O formation, XRD results of CZ samples, in situ DRIFTS of Pd/CZN12 and Pd/CZ12. See DOI: 10.1039/x0xx00000x

analysis of X-ray diffraction (XRD) patterns, UV-Raman, XPS, OSC, Pd-dispersion and in situ DRIFTS.

2. EXPERIMENTAL

2.1 Catalyst preparation

The CeO_2-ZrO_2-Nd_2O_3 mixed oxides samples were prepared by a conventional coprecipitation method combined with supercritical drying technique. The detailed process was conformed to literature.[21] The additive content of Nd_2O_3 was 5.0 wt. % and the theoretical molar ratios of CeO_2/ZrO_2 was 4/1, 3/1, 2/1, 1/1, 1/2, 1/3, and 1/4, respectively. The fresh supports were calcined at 500 °C for 4 h in static air and referred to as CZN41, CZN31, CZN21, CZN11, CZN12, CZN13, and CZN14. A portion of each support was further aged at 1100 °C for 4 h and denoted as CZN41a, CZN31a, CZN21a, CZN11a, CZN12a, CZN13a, and CZN14a, correspondingly. The corresponding Pd/CZN catalysts (Pd content was 0.5 wt.%) were prepared by a conventional impregnation method with an aqueous of H_2PdCl_4 as metal precursor. The fresh catalysts were labeled as Pd/CZN41, Pd/CZN31, Pd/CZN21, Pd/CZN11, Pd/CZN12, Pd/CZN13, and Pd/CZN14. Ceria-zirconia supports (without Nd) and the corresponding catalysts were also prepared with the same method as stated above and the CeO_2/ZrO_2 molar ratio of 4/1, 2/1, 1/1, 1/2 and 1/4. The Nd-free support was referred to as CZ41, CZ21, CZ11, CZ12 and CZ14, and the catalysts were labled as Pd/CZ11 and Pd/CZ12. All the catalysts were calcined at 1100 °C in air for 4 h in order to investigate the thermal stability property, and the corresponding aged catalysts were labeled as Pd/CZN41a, Pd/CZ31a, Pd/CZN21a, Pd/CZN11a, Pd/CZN12a, Pd/CZN13a, Pd/CZN14a and Pd/CZ12a, respectively.

2.2 Catalytic activity tests

The catalytic activity tests were carried out in a fixed-bed continuous flow reactor. 0.2 ml catalyst (0.3–0.45 mg) was used. The feed stream composed of 0.12% NO, 0.03% NO_2, 0.066% C_3H_6, 0.033% C_3H_8, 0.6% CO, and 0.745% O_2 with the balance Ar at a GHSV of 43,000 h^{-1}, analyzed by on-line FTIR spectrometer (Bruker EQ55) coupled with a multiple reflection transmission cell (Infrared Analysis Inc., path length 10.0 m) before and after the simulated exhaust gas passed through the reactor.

The air/fuel ratio (λ) was defined as $\lambda = (2V_{O_2} + V_{NO} + 2V_{NO_2})/(V_{CO} + 9V_{C_3H_6} + 10V_{C_3H_8})$ (V is the concentration of each gas in units of volume percent) and λ = 1 was used in all the activity measurements. The static operational window experiments were carried out at 400 °C with different λ values (0.9 ~ 1.15) by adjusting the concentration of O_2. The in situ dynamic operational window experiments were carried out at 400 °C by adjusting the concentration of O_2 and analyzed by a Hiden QIC-20 mass detector working in electron impact (EI) mode at 70 eV. The NO_x operational window was measured when the λ is adjusted from 1.0 to 1.15, while the HC/CO operational window was measured when the λ is adjusted from 1.0 to 0.8.

2.3 Characterization techniques

The crystal structure of the CZN samples was confirmed by powder X-ray diffraction (XRD) using CuK_α radiation (BRUKER D8 Advance, Bruker Co., German). The XRD data for Rietveld analysis were collected over the range of 10 – 120° (2θ) with a step size of 0.02° and a count time of 3 s. The Rietveld refinement was performed using the Jade 7.0 program, and a pseudo-Voigt profile function with preferred orientation was used.

UV-Raman spectra were recorded on a Raman spectrograph with He-Gd laser of 325 nm excitation wavelength. The spectral resolution was 4 cm^{-1}, and the spectra acquisition consisted of 2 accumulations of 30 s for each sample. A frequency range of 100–1000 cm^{-1} was observed.

X-ray photoelectron spectroscopy (XPS) experiments were performed on a PHI5000c spectrometer with the Mg Kα radiation (1253.6 eV) operating at 14 kV and 20 mA. The binding energies were calibrated with the C_{1s} level of adventitious carbon (284.6 eV) as the internal standard reference.

The oxygen storage capacity (OSC) was measured using pulse injection technique until no consumption of oxygen was detected with a CHEMBET-3000. The sample was reduced with a flow of 10 ml/min H_2 at 550 °C for 1 h, then cooled down to 400 °C and purged by helium stream.

Pd dispersion was determined by CO chemisorption at room temperature, using a CHEMBET-3000 (Quantachrome Co.). Prior to the experimental trials, each sample was reduced under a flow of 5% H_2/95% N_2 at 400 °C for 1 h and then purged with He at the same temperature for 0.5 h. The sample was subsequently cooled to room temperature under a He flow and maintained at this temperature for another 0.5 h. Finally, CO pulses were injected into the sample bed every 5 min until no further consumption of CO could be detected.

Diffuse Reflectance Infrared Fourier Transform Spectroscopy (DRIFTS) experiments were performed with a Nicolet 6700 FTIR spectrometer with an MCT detector, a DRIFTS cell fitted with CaF_2 windows and a heated reaction chamber. Spectra were collected after average of 32 scans at the resolution of 4 cm^{-1}. Catalysts were pretreated in Ar at 450 °C for 0.5 h and then cooled down to 30 °C. The composition and flow rate of feed stream were kept constant through the test.

3. RESULTS AND DISCUSSIONS

3.1 Catalytic performance of the catalysts

Fig. 1 presents the light-off curves of HC, CO, NO and NO_2 under simulated reaction condition (CO + HC + NO_x + O_2) over fresh Pd/CZN and Pd/CZ11 catalysts. The addition of Zr clearly improves the catalytic activity of HC and NO conversions, especially when lowering CeO_2/ZrO_2 molar ratios to 1/4. However, Pd/CZN12 and Pd/CZN11 show the best catalytic activity of CO and NO_2, respectively. In the Zr-rich region, the catalytic activity of CO and NO_2 conversions notably decreases

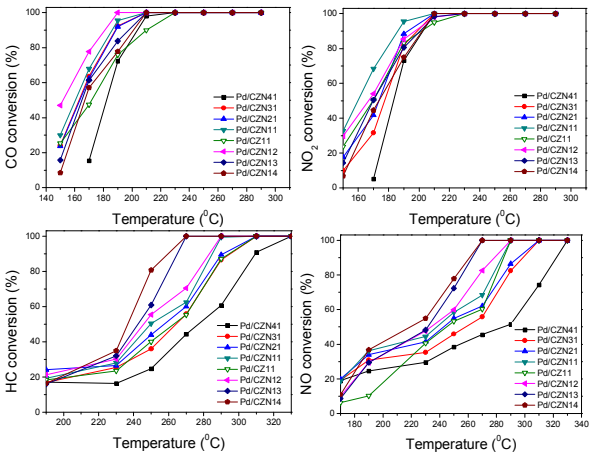

Fig. 1 Three-way conversion over the fresh Pd/CZN and Pd/CZ11 catalysts

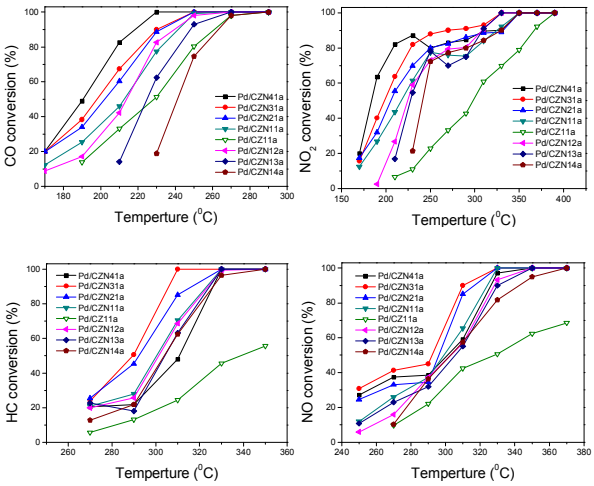

Fig. 2 Three-way conversion over the aged Pd/CZNa and Pd/CZ11a catalysts

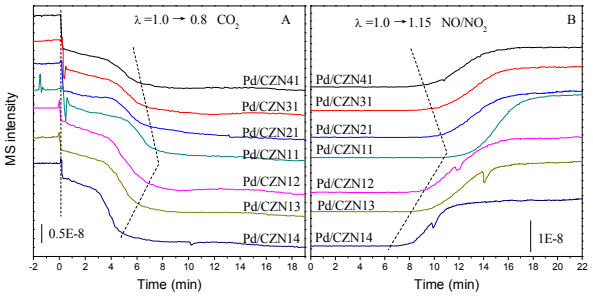

Fig. 3 The in situ dynamic operational window of CO, HC (A) and NO_x (B) over the fresh Pd/CZN catalysts at 400 °C

when increasing the Zr content. Fig. 2 presents the conversions of HC, CO, NO and NO_2 over aged catalysts calcined at 1100 °C. The deteriorated structure and sintering of active components cause a drop in catalytic activity compared with the fresh catalysts.[22, 23] Different from fresh catalysts, aged catalysts exhibit sharply decreased catalytic activity of CO with the increased Zr content. Pd/CZN41a catalyst displays the lowest full-conversion temperature for CO oxidation, while Pd/CZN31a catalyst shows the highest catalytic activity for HC, NO2 and NO eliminations. Zr-rich Pd/CZNa catalysts with CeO_2/ZrO_2 molar ratio from 1/1 to 1/4 exhibit very similar catalytic performance for HC, NO_2 and NO elimination. Besides, Pd/CZN11 shows much better catalytic activity over all the target pollutants compared to Nd-free catalysts (Pd/CZ11), especially for the aged catalysts, proving that the appearance of Nd shows an enhancement on the catalytic performance of catalysts.

The selectivity of N_2O formation over the fresh catalysts is also investigated and the results are displayed in Fig. 1S. It can be seen that N_2O is the main N-containing product during cold start process. However, the N_2O selectivity is sharply reduced when the reaction temperature reaches 230 – 250 °C, which is the light-off temperature of NO reduction. Moreover, the N_2O selectivity of each catalyst decreases with the increasing Zr addition and Pd/CZN14 exhibits the lowest selectivity of N_2O, indicating that the introduction of Zr promotes the reduction performance of NO_x. Besides, the amount of N_2O formation over Pd/CZ11 is similar with that over Pd/CZN11, indicating that the Nd addition doesn't work on the improvement of selectivity.

In an attempt to analyse the dynamic behaviour of the Pd/CZN system, we investigate the dynamic operational windows and the results are shown in Fig. 3. Fig. 3A shows the CO_2- time curves (O_2 concentration are adjusted from λ = 1 to λ = 0.8), while the Fig. 3B shows the NO_x - time curves (O_2 concentration are adjusted from λ = 1 to λ = 1.15). The longer time for NO_x and CO_2 to achieve a balance, the wider operational window it indicates.[24] It is obvious that Ce-rich catalysts exhibit wider operational window than Zr-rich catalysts and Pd/CZN11 shows the best catalytic behaviour under dynamic conditions.

To obtain more information about the influence of CeO_2/ZrO_2 molar ratios on the structural/textural properties of CZN supports, which may be responsible for enhancing the catalytic performance, Rietveld analysis of XRD patterns, UV-Raman, XPS, OSC, Pd-dispersion and in situ DRIFTS results obtained for the catalysts are analysed below.

3.2. Structural characterization

3.2.1 XRD

Fig. 4A shows the XRD patterns of the fresh CZN supports with various CeO_2/ZrO_2 molar ratios. The patterns comprise peaks from two phases: cubic and tetragonal. Peaks of pure neodymium and zirconia can't be detected indicating the

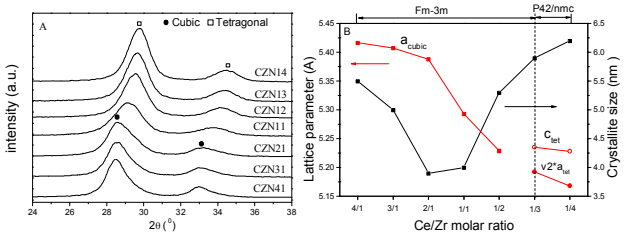

Fig. 4 XRD patterns of CZN supports calcined at 500 °C (A); the corresponding lattice parameter and crystallite size (B)

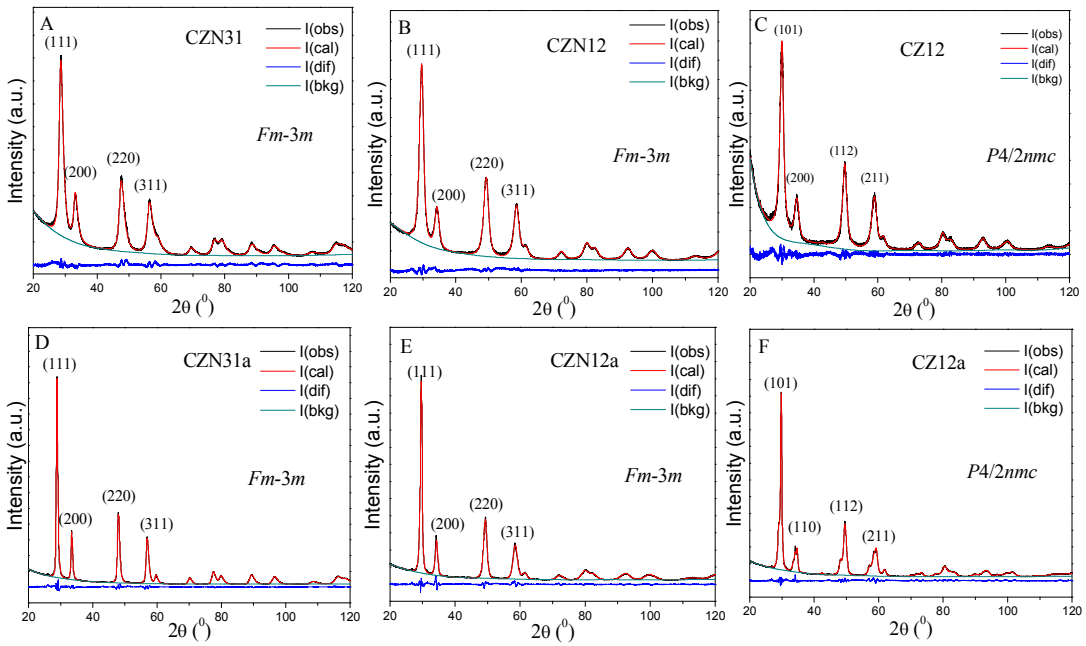

Fig. 5 Rietveld analysis of XRD patterns of CZN31 (A), CZN12 (B) and CZ12 (C) samples prepared at 500 ^{0}C and the CZN31a (D), CZN12a (E) and CZ12a (F) samples prepared at 1100 ^{0}C. The Miller indices of the most intense peaks of cubic and tetragonal phases are indicated. Differences between observed and calculated intensities are included at the bottom of the figure.

Table 1 *R*-factors (R_{wp} and R_p), goodness-of-fit indicator (χ^2), thermal factors (B_{iso}) and structural parameters deduced from Rietveld refinement of the XRD patterns for the supports.

Samples	CZN31	CZN12	CZ12	CZN31a	CZN12a	CZ12a
S.G.	*Fm*-3*m* (225)	*Fm*-3*m* (225)	$P4_2/nmc$ (137)	*Fm*-3*m* (225)	*Fm*-3*m* (225)	$P4_2/nmc$ (137)
Atom	O	O	O	O	O	O
Sites	8c	8c	4d	8c	8c	4d
Occupation	0.963(2)	0.946(1)	1.003(30)	0.928(2)	0.934(2)	0.952(11)
B_{iso}	3.29	2.49	1.57	1.44	1.56	-0.30
V/Å^3	158.6	143.0	71.4	154.9	143.5	70.1
a/Å	5.4130(4)	5.2299(4)	3.6799(6)	5.3709(2)	5.2350(4)	3.6522(2)
c/Å			5.2735(15)			5.2544(4)
R_p	3.99	3.82	3.88	4.27	3.99	4.12
R_{wp}	5.01	4.79	5.34	4.99	5.43	5.31
χ^2	1.58	1.57	1.90	1.37	1.85	1.66

incorporation of Nd and Zr dopant cations into ceria lattice.[8] As shown in Fig. 4, the characteristic diffraction peaks between 20^o and 40^o shift to higher 2θ degrees and the lattice parameter decreases with the increasing Zr content. According to literature[25], the substitution of Ce^{4+} cation (0.097 nm) by Zr^{4+} cation (0.084 nm) would favour the crystalline contraction structure and thus decrease the lattice parameter. So, the results indicate the insertion of Zr into the CeO_2 lattice. From Fig. 4A, it is obviously that the shift of peaks is not similar. Ce-rich supports display almost the same diffraction peaks, and the lattice parameters of the CeO_2 fluorite structure slightly decrease as the Zr content increases (Fig. 4B, CeO_2/ZrO_2 = 4/1 ~ 2/1). However, when CeO_2/ZrO_2 ratio ≤ 1/1, the ZrO_2 becomes the dominant factor of the phase nature thus causing a sharply decline of the lattice parameter and shifting the peaks to much higher 2θ degree. Phase transition occurs when CeO_2/ZrO_2 molar ratio further decreases to 1/3 and 1/4, and diffraction peaks of tetragonal phase are detected (Fig. 4A). From Fig. 4B, it can be seen that the crystal size of the supports decreases when CeO_2/ZrO_2 decreases to 2/1 (3.9 nm) and 1/1 (4.0 nm), but increases with increasing Zr content after that, indicating that CZN support with CeO_2/ZrO_2 molar ratio around 1/1 owns the most homogeneous ternary structure, corresponding to the smallest crystal size. The XRD patterns of the fresh CZ supports with several CeO_2/ZrO_2 molar ratios are displayed in Fig. 2S, along with the calculated lattice parameters (Table 1S). From these results, we can clearly notice that the phase segregation occurs from CeO_2/ZrO_2 of 2/1 on the Nd-free samples and their crystal sizes are larger than the corresponding Nd-doping samples. As we know that Nd^{3+} (0.112 nm) has larger ion radius than Zr^{4+} (0.084 nm), which will cause the lattice deformation of tetragonal phase to

form a pseudocubic structure.[26, 27] Therefore, the introduction of neodymia into CeO_2-ZrO_2 solid solutions could lead to the expansion of CeO_2-ZrO_2 lattice and stabilization of cubic modification. The formation of stabilized ternary CeO_2-ZrO_2-Nd_2O_3 structure can effectively enhance the structural homogeneity of support, which leads to the better catalytic activity of Pd/CZN11 catalysts compared with Pd/CZ11.

To further investigate the structural changes, generated by the insertion Zr and Nd, the Rietveld analysis of CZN31, CZN12 and CZ12 samples was carried out as examples. The refinement of XRD patterns of these three samples was performed using cubic and tetragonal models. The Rietveld's method has given a reasonable fit of the diffraction profiles (R_{wp} < 6%, χ^2 < 2), and thermal factors were fixed to those of the pure phases. In Fig. 5, the XRD pattern of CZN31 and CZN12 display diffraction peaks of fluorite structure with space group of *Fm*-3*m*, but tetragonal phase (S.G. $P4_2/nmc$) is the unique detected phase for CZ12 sample.

The structural parameters are presented in Table 1. For the fresh support, Zr insertion causes the shrinkage of lattice parameter from 5.4130 nm to 5.2299 nm and unit cell volume from 158.6 Å^3 to 143.0 Å^3 when CeO_2/ZrO_2 molar ratio decreases from 3/1 to 1/2, due to the substitution of Ce^{4+} (0.97 Å) by Zr^{4+} ions (0.84 Å).[28] Comparing CZ12 with CZN12, the Nd-free sample shows smaller unit cell volume (71.4 Å^3) because of the phase change. Moreover, structural site occupancies have also been analyzed in different crystalline phases. The occupancy of O in CZN12 sample (0.946) is much smaller than CZ12 (1.003) indicating more oxygen vacancies formed in the CZN12 support. It is because that the incorporation of Nd into CeO_2-ZrO_2 lattice leads to the expansion of the lattice and thus enhances lattice defect, which increases the oxygen vacancies and improves lattice oxygen mobility. Meanwhile, the occupancy of O in CZN31 sample is 0.963, larger than that in CZN12 (0.946). For the increase of oxygen vacancies accelerates the oxygen mobility in support and thus promotes the catalytic activity of Pd/CZN catalysts, the catalytic activity of HC and NO over Pd/CZN12 catalyst is better than that over Pd/CZN31 catalyst, as displayed in Fig.1. After high temperature treatment, the sintering of CZN support results in the formation of larger crystallite as revealed by the sharply increased intensity of diffraction peaks and more sharpened peak pattern. In spite of this, CZN12a remains the cubic phase, indicating the good thermal stability of Nd-doped CZ support compared with CZ12a. However, the occupancy of O in CZN12a sample (0.934) is larger than that in CZN31a (0.928), indicating that more oxygen vacancies are formed in CZN31a than in CZN12a, which is in accordance with the better catalytic performance of Pd/CZN31a (Fig. 2).

3.2.2 UV-Raman

Raman spectroscopy is dominated by oxygen lattice vibrations and it is sensitive to the crystal symmetry, thus being a sufficiently powerful way to analyze structural properties of nanomaterials. Fig. 6 shows the UV Raman (λ_{ex} = 325 nm) spectra of fresh and aged supports. As shown in Fig. 6, four main peaks at 324 (δ), 447 (α), 545 (β) and 640 (γ) cm^{-1} are existed, as observed in literatures.[19, 29-32] Peak α is assigned to the F_{2g} mode vibration of cubic fluorite structure. The increase of Zr content leads to a decrease in the intensity of peak α, indicating the decrease of cubic structure phase. When CeO_2/ZrO_2 molar ratio reaches 1/2, peak α almost disappears, demonstrating the phase changes of supports. The weak peak δ is related to the presence of metastable t'' phase, which is an intermediate phase between t' and cubic CeO_2.[33] Band at around 500-650 cm^{-1} contains two peaks: one centers on 545 cm^{-1} (peak β), while the other is at around 620 cm^{-1} (peak γ). Peak β is attributed to surface oxygen vacancies due to the charge compensation mechanism. Peak γ can be split into two possible species: γ_1 and γ_2. Peak γ_1 is assigned to the formation of O_h symmetry that includes a dopant cation in 8-fold coordination of O^{2-} (ZrO_8-type complex) containing very few oxygen vacancies. Peak γ_2 predicts the possibility of a stable t-phase in the mixed oxide system with increasing Zr content. As observed in these figures, Zr doping remarkably altered the shape of the spectra. Thus, we focused on peak α, β and γ to investigate the defect contributions. Fig. 7 shows plots of $I_\beta/(I_\alpha+I_\beta+I_\gamma)$% (denoted as v_β, the relative concentration of O^{2-} vacancies) and $I_\gamma/(I_\alpha+I_\beta+I_\gamma)$% (denoted as v_γ, the relative concentration of ZrO_8-type complex or t-phase) versus the CeO_2/ZrO_2 molar ratio, where I_α, I_β, and I_γ correspond to the maximum intensities of peak α, β and γ. Additionally, v_γ/v_β reflects the relative concentration between the two types of defect complexes.

As can be seen in Fig. 7A, v_γ almost remains constant when CeO_2/ZrO_2 ration decreases from 4/1 to 2/1 and then rapidly increases when CeO_2/ZrO_2 ratio ≤ 1/1. Combined with the lattice parameter results (Fig. 4B), it demonstrates that the impact of Zr dopant on the structure of Ce-rich supports is small, while when ZrO_2 becomes the dominant factor, it will have a great influence on the structure. On the other side, v_β slightly increases until CeO_2/ZrO_2 molar ratio decreases to 1/2, indicating that the addition of moderate ZrO_2 can increase

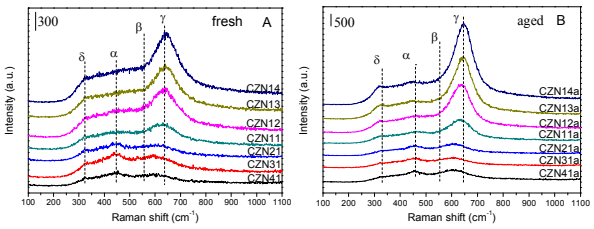

Fig. 6 The UV-Raman (λ_{ex} = 325 nm) spectra of fresh (A) and aged (B) supports

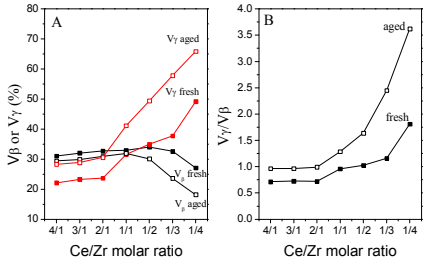

Fig. 7 v_β, v_γ and v_γ/v_β ratio of CZN supports with different CeO_2/ZrO_2 molar ratio

Table 2 Surface elemental composition and oxidation state of Ce measured by XPS

Sample	Surface composition (at.%)				Ce/Zr ratio	Nd/Ce+Zr ratio (10^{-2})	Ce^{3+} in Ce (%)
	Ce 3d	Zr 3d	Nd 3d	O 1s			
Pd/CZN41	17.79	4.54	0.24	77.43	3.92	1.07	19.8
Pd/CZN21	15.24	8.18	0.24	76.34	1.86	1.02	22.1
Pd/CZN11	11.44	12.75	0.25	75.56	0.90	1.03	25.1
Pd/CZN12	7.87	16.81	0.20	75.12	0.47	0.81	26.9
Pd/CZ12	8.08	16.82	-	71.57	0.48	-	23.9
Pd/CZN14	4.57	20.2	0.18	75.05	0.23	0.73	29.0
Pd/CZN41a	15.77	4.74	0.51	78.98	3.33	2.49	17.1
Pd/CZN21a	12.23	8.32	0.40	79.05	1.47	1.95	19.2
Pd/CZN11a	9.60	11.2	0.40	78.80	0.86	1.92	22.7
Pd/CZN12a	5.06	15.01	0.26	79.67	0.34	1.30	25.0
Pd/CZ12a	5.91	15.33	-	78.67	0.39	-	22.1
Pd/CZN14a	3.95	19.35	0.24	76.46	0.20	1.03	26.2

Table 3 OSC values over CZN supports, the width of the static operational window (ΔW) and Pd-dispersion for the corresponding catalysts with different CeO_2/ZrO_2 molar ratios

Samples	OSC (umol/g) [a]		ΔW		Pd dispersion (%)[b]		Pd particle size (nm)[c]	
	fresh	aged	fresh	fresh	fresh	aged	fresh	aged
Pd/CZN41	402.7	297.6	0.10	0.10	15.82	9.16	7.04	12.16
Pd/CZN31	464.0	324.8	0.13	0.10	20.48	10.73	5.44	10.38
Pd/CZN21	490.4	419.3	0.15	0.11	16.30	8.93	6.83	12.47
Pd/CZN11	550.7	468.9	0.12	0.11	11.76	8.81	9.47	12.64
Pd/CZN12	504.9	380.1	0.12	0.10	8.82	4.44	12.63	25.08
Pd/CZN13	440.9	331.2	0.10	0.09	7.76	3.94	14.35	28.27
Pd/CZN14	389.2	325.9	0.10	0.07	7.52	2.42	14.81	46.02

[a] The amount of O adsorbed on CZN supports.

[b] Calculated supposing the adsorption of one CO atom with one Pd atom.

[c] Calculated using equation d (nm)= 6 * 10^5 * M_{Pd} / (ρ_{Pd} * Pd dispersion * S_{Pd}), With M_{Pd}, molar weigh of palladium (106.42 g/mol); ρ_{Pd}, palladium density (12 g/cm^3); S_{Pd}, molar surface area of palladium assuming an equidistribution of the low index faces (S = 47,780 m^2/mol for Pd metal).[34]

both two defects. However, phase transition occurs on CZN13 and CZN14 (Fig. 4), leading to the decrease of oxygen vacancies, demonstrating that the excess Zr content may lead to exhibits the formation of oxygen vacancies. It is in accord with the result of good catalytic performance of CO and NO_2 over Pd/CZN catalysts with CeO_2/ZrO_2 molar ratio of 1/1 ~ 1/2. For the aged samples, v_β decreases a little compared with fresh supports among Ce-rich CZN supports. When CeO_2/ZrO_2 ratio ≤ 1/1, v_β value falls into decline, which is bad for the catalytic performance of the corresponding Zr-rich catalysts. The v_γ/v_β value of aged samples is much higher than that of fresh samples, suggesting that either the ZrO_8-type defect sites or the t-phase enriches on the surface after the high temperature treatment. Defects in Zr-doped CeO_2 have been extensively studied by Luo et al.[29] Following their experimental work, the increased calcination temperature leads to more perfect lattice and increasing ordering level, which results in the decline of the ZrO_8-type defect sites. So the increase of v_γ/v_β ratio mainly indicates the formation of more stable t-phase after aged, which in turn reduces the concentration of oxygen vacancies, as can be seen in Fig. 7A. It is worth noting that CZN12a displays tetragonal structure in UV-Raman results, which is contrary to the results of XRD (Fig. 5 and Table 1). According to the literature,[35] the UV-Raman signals are mostly from the surface region of the support due to the strong absorption of the samples while the XRD results are related to the bulk of the support, and the phase transformation of ZrO_2 is a process from the surface region to the bulk, indicating that the tetragonal phase is initially formed at the surface of CZN12a supports, which mainly exhibit cubic phase in the bulk. Besides, for the aged samples, the change regularities of both strength and shift are similar with the fresh samples and no characteristic features of ZrO_2 and Nd_2O_3 are found before and after aged, indicating that the surface structure of supports is homogeneous and stable.

3.2.3 XPS

The composition of the outermost surface layers is investigated by XPS and the related data are presented in Table 2. Pd can't be observed due to the extremely low metal loading content (0.5 wt. %). For fresh catalysts, the surface atom ratios of CeO_2/ZrO_2 are a little smaller than the theoretical atomic ratios, which means the outer part is enriched with Zr to a small content. For Pd/CZ12 catalyst, the surface atom ratio of CeO_2/ZrO_2 (0.48) is higher than that of Pd/CZN12 (0.47), demonstrating that part of Ce atoms of the

surface layer is replaced by Nd. The diffusion of Nd atom from surface to the bulk of the catalysts can be noticed when increasing the Zr content, suggesting the insertion of Nd into the ceria lattice and demonstrating that the appropriate Zr content may facilitates the formation of more homogeneous Ce-Zr-Nd-O ternary solid solution. As being discussed in XRD results, the substitution of Ce by Nd leads to the expansion of the lattice and thus increases the oxygen vacancies and accelerates the oxygen mobility. So the diffusion of Nd with the increasing Zr content helps to enhance the OSC of support, which improves the catalytic activity of the corresponding catalysts. An enrichment of Nd and Zr can be observed after aging process, proving the sintering of support. The surface Ce^{3+}/Ce^{4+} ratio increases when increasing the Zr content and the ratio in Pd/CZ12 (23.9, 22.1) is much less than that in Pd/CZN12 (26.9, 25.0), indicating that the incorporation of ZrO_2 and Nd_2O_3 may promote the reduction of Ce^{4+} to Ce^{3+}. It is well known that the formation of oxygen vacancies lead to the presence of Ce^{3+} according to the electroneutrality condition. So, in other words, Zr and Nd dopants both can increase the relative concentration of oxygen vacancies, which is beneficial for the NO reduction.[36]

3.2.4 Pd-dispersion, OSC and static operational window

The OSC value is regarded as one of the important influence on the width of the operational window for three-way catalysts. Among the Ce-rich supports, OSC value increases with the increased Zr content and CZN11 displays highest OSC value before and after aged (550.7 and 468.9 μmol/g, respectively). Additionally, the OSC values of fresh and aged CZ12 samples are 363.8 and 304.0 μmol/g, much smaller than that of CZN12 samples, proving that Nd insertion helps to increase the OSC value. Zr has a lower coordination number within the ceria lattice and thus increases bulk oxygen mobility, resulting in the enhanced oxygen storage property.[20] When $CeO_2/ZrO_2 \leq 1/1$, the OSC value notably decrease. According to the literature, the overall degree of reduction of CeO_2 is limited in the $M_xCe_{1-x}O_{2-x/2}$ type, which means that less oxygen vacancies in total amount are needed to achieve a certain degree of non-stoichiometry compared to pure CeO_2.[18] So the massive decrease of Ce content in support lower the amount of oxygen vacancies, leading to the decrease of OSC value. The change regularity of OSC value is almost the same with the in situ dynamic operational window, demonstrating that the in situ dynamic operational window is basically affected by OSC value. For the fresh catalysts, the effect of OSC values does reflect in the elimination of CO and NO_2: catalysts with higher OSC value exhibit better catalytic performance of CO and NO_2. However, we cannot find the closely relationship between the catalytic activity of HC or NO and OSC values, indicating that OSC isn't the main factor to influence the HC and NO conversions.

We also evaluated the conversions of CO, HC and NO_x under different air/fuel ratios (λ) at 400 °C over fresh and aged catalysts. ΔW (static operational window) acts as a scale to evaluate catalyst property when CO, HC and NO_x conversions all reach to 90% under rich and lean conditions. The wider the ΔW value is, the broader the three-way operational window is. ΔW value first increases when CeO_2/ZrO_2 molar ratio reaches 2/1 and then decreases when further increasing the Zr content. Catalysts with CeO_2/ZrO_2 molar ratio from 4/1 to 1/2 display larger ΔW value before and after aged, indicating that only the addition of appropriate Zr can improve the catalytic performance and the thermal stability of catalysts. Additionally, the result is different from the dynamic performance (Fig. 3). In this dynamic condition, the result is directly related to oxygen storage capacity, while the ΔW value may be based on the metal and metal-promoter interface behaviours besides the OSC value.

It is generally recognized that the Pd dispersion and Pd particle size may have a great influence on the catalytic activity of CO, NO_x and HC eliminations, so the Pd dispersion was investigated by CO chemisorption and the corresponding Pd particle size were also calculated. CeO_2 may cause additional metal-support interaction,[37] thus higher Pd dispersions have been observed for Ce-rich catalysts, and CZN31 displays the highest Pd dispersion as well as the smallest Pd particle size. According to the literature,[23] the main factors affecting the CO catalytic activity are the Pd-dispersion and the number of Pd-CZ interface. As shown in Table 3, the Pd particle size increases with the increasing Zr content, suggesting the weakened Pd-support interaction and the formation of larger Pd particles at the surface, which leads to the decreased CO catalytic activity. On the contrary, NO reduction is structure-sensitive and prefers to be dissociated on large particle size of Pd. Meanwhile, steps of synchronous C-H and N-O dissociation seem to be more predominant than the simple HC oxidation by lattice O or active O_2,[38] indicating that relatively large Pd particle may improve the catalytic activity for NO and HC conversions. Thus, fresh Pd/CZN14 catalyst shows the best catalytic performance for NO and HC eliminations due to its largest Pd particle size. However, the presence of oxygen vacancies associated with the Ce^{3+} ions near the noble metal particles in CZ-supported catalysts has been indicated as the driving force for NO dissociation.[36] So, for the aged samples, the decreased concentration of oxygen vacancies in aged Zr-rich support (UV-Raman, Fig. 7) is the main factor to lead to the decreased catalytic activity of NO and HC conversions when increasing the Zr content.

3.2.5 In situ DRIFTS

It is necessary to consider the temperature and structure dependences of adsorption/activation competition processes between the different reactants. To obtain an integrated understanding of the formation and disappearance of surface species during the redox process of each target pollutant, fresh Pd/CZN and Pd/CZ12 catalysts were tested by in situ DRIFTS at 50 and 270 °C (Fig. 8). For the Zr doping can significantly affect the electronic properties and the geometrical configuration of sorption species on ceria surfaces, the observed frequencies related to the surface species are expected to change when increasing Zr content.[39] Unfortunately, species adsorbed on Pd can be hardly observed because of the extremely low metal loading content (0.5 wt.%).

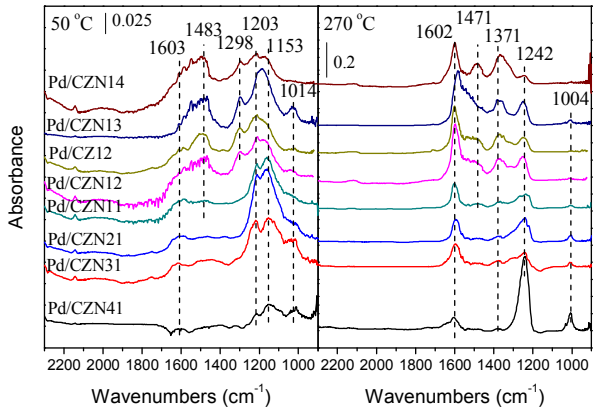

Fig. 8 DRIFTS spectra collected at 50 and 270 °C during exposure of fresh Pd/CZN and Pd/CZ12 catalysts to stoichiometric CO + HC + NO_x + O_2 reaction conditions.

At 50 °C, the spectra are mainly dominated by the presence of bidentate nitrites adsorbed on CeO_2 (1153 cm^{-1}) and ZrO_2 (1203 cm^{-1}), and the bidentate Zr^{4+}=O_2N species increases progressively as the increasing Zr content. Weak bands assigned to the bidentate/monodentate nitrates species adsorbed on ZrO_2 develop at 1603-1483, 1298 and 1014 cm^{-1} over Zr-rich catalysts.[39, 40] The main pathway to form nitrate species on CeO_2-ZrO_2-based mixed oxides is the reaction of nitrite species with an O^* active species. The O^* active species on surfaces is mainly of superoxide O_2^- type which is formed through electron transfer by one-electron surface defects.[41] As stated in UV-Raman results, the incorporation of Zr increases the defects on the surface of sample and thus increases the concentration of O^* active species, leading to accelerate the formation of nitrate species.

As for the catalytic activity results (Fig. 1), all the catalysts have already reached their light-off temperature ($T_{50\%}$) when the reaction temperature increases to 270 °C, except for Pd/CZN41. So we choose 270 °C to study the adsorption and active of target pollutants at high temperatures. As shown in Fig. 8, Pd/CZN41 catalyst shows an obviously different spectra with strong intensity of bands related to nitrate species (1602, 1242 and 1004 cm^{-1}) when reaction temperature reaches 270 °C, which is in accord with its relatively worse NO_x catalytic performance. However, the intensity of band at 1242 cm^{-1} decrease significantly when increasing the Zr content, and band at 1013 cm^{-1} almost disappears for Pd/CZN14 catalyst, revealing the elimination of nitrate species. Meanwhile, some new bands in the region of 1600-1300 cm^{-1} can be clearly identified when Zr content further increases to CeO_2/ZrO_2 = 1/2, which may be attributed to formate/acetate/carbonate species adsorbed on CZN supports, indicating that reactions involving HC oxidation become significant at Zr-rich catalysts.[42-44] The in situ DRIFTS spectra of Pd/CZN12 and Pd/CZ12 collected at different temperatures are displayed in Fig. 3S. Their spectra are very similar with each other, because these spectra mainly reflect the adsorption of species on Ce or Zr site while the insertion of 5 wt. % Nd doesn't change these sites a lot.

4. CONCLUSIONS

To analyze the doping effect of Nd_2O_3 on structure-activity relation in CeO_2-ZrO_2 structure, a series of CeO_2-ZrO_2-Nd_2O_3 (CZN) mixed oxides with different CeO_2/ZrO_2 molar ratios have been synthesized and the corresponding Pd/CZN catalysts were prepared by impregnation method. Through the Rietveld analysis of CZN31, CZN12 and CZ12 using XRD data, we find that the incorporation of Nd into CeO_2-ZrO_2 structure will cause the expansion of the lattice and thus effectively stabilize the cubic structure. The occupancy of O in CZN12 sample (0.946) is much smaller than CZ12 (1.003), which implies that the addition of Nd enhances lattice defect, leading to increase the oxygen vacancies and improve lattice oxygen mobility. Among the Nd-doped catalysts, UV-Raman results display a homogeneous and stable ternary structure. The increase of oxygen vacancies will increase the concentration of O^* active species, leading to accelerate the formation of nitrate species. Combined with the Pd-dispersion results, the increase of Zr content also enlarges the Pd particle size, where NO prefers to be dissociated. So the increase of Zr content for the fresh catalysts enhances the catalytic activity of NO_x elimination. Meanwhile, steps of synchronous C-H and N-O dissociation seem to be the predominant step for HC conversion. Thus, fresh Pd/CZN14 catalyst shows the best catalytic performance for NO and HC eliminations. For the aged catalysts, the decreased concentration of oxygen vacancies and the enrichment of tetragonal phase on the surface of Zr-rich support (UV-Raman, Fig. 7) is the main factor to lead to the decreased catalytic activity of NO and HC conversions. Moreover, the main factors affecting the CO catalytic activity are the Pd-dispersion and the number of Pd-CZ interface. The Pd-dispersion decreases with the increasing Zr content, leading to the decreased CO catalytic activity, especially for the aged catalysts. Among the Ce-rich supports, an enhancement of relative OSC value is observed with increasing Zr content, and CZN11 displays highest OSC value before and after aged (550.7 and 468.9 umol/g, respectively). When further increasing Zr content, a drop of OSC value occurs due to the massive reductions of Ce content. The change regularity of OSC value is almost the same with the in situ dynamic operational window, demonstrating that the in situ dynamic operational window is basically affected by OSC value. However, catalysts with CeO_2/ZrO_2 molar ratio from 4/1 to 1/2 display wider static operational window, indicating that an excess amount of Zr will decrease the catalytic activity.

Acknowledgements

The authors are thankful to Prof. Lv Guanglie of Zhejiang University for his assistance in XRD Rietveld analysis. This work was supported by Nature Science Foundation of China (No.: 21477109).

References

1 M. Pijolat, M. Prin, M. Soustelle, O. Touret and P. Nortier, Journal of the Chemical Society, Faraday Transactions, 1995, 91, 3941-3948.
2 M. Shelef and R. W. McCabe, Catalysis Today, 2000, 62, 35-50.
3 S. Colussi, A. Gayen, M. Farnesi Camellone, M. Boaro, J. Llorca, S. Fabris and A. Trovarelli, Angew Chem Int Ed Engl, 2009, 48, 8481-8484.
4 S. A. Venâncio and P. E. V. de Miranda, Ceramics International, 2011, 37, 3139-3152.
5 S. Damyanova, C. A. Perez, M. Schmal and J. M. C. Bueno, Applied Catalysis A: General, 2002, 234, 271-282.
6 J. R. González-Velasco, M. A. Gutiérrez-Ortiz, J.-L. Marc, J. A. Botas, M. P. González-Marcos and G. Blanchard, Applied Catalysis B: Environmental, 1999, 22, 167-178.
7 X. Yang, L. Yang, S. Lin and R. Zhou, Chinese Journal of Catalysis, 2014, 35, 1267-1280.
8 A. Papavasiliou, A. Tsetsekou, V. Matsouka, M. Konsolakis, I. V. Yentekakis and N. Boukos, Applied Catalysis B: Environmental, 2009, 90, 162-174.
9 J. G. Mira, V. R. Pérez and A. Bueno-López, Catalysis Today, 2015, 253, 77-82.
10 J. Wang, M. Shen, Y. An and J. Wang, Catalysis Communications, 2008, 10, 103-107.
11 P. Vidmar, P. Fornasiero, J. Kaspar, G. Gubitosa and M. Graziani, Journal of Catalysis, 1997, 171, 160-168.
12 H. He, H. X. Dai, K. W. Wong and C. T. Au, Applied Catalysis a-General, 2003, 251, 61-74.
13 Q. Wang, G. Li, B. Zhao, M. Shen and R. Zhou, Applied Catalysis B: Environmental, 2010, 101, 150-159.
14 B. Zhao, Q. Wang, G. Li and R. Zhou, Journal of Environmental Chemical Engineering, 2013, 1, 534-543.
15 L. Yang, S. Lin, X. Yang, W. Fang and R. Zhou, Journal of hazardous materials, 2014, 279, 226-235.
16 Q. Wang, G. Li, B. Zhao and R. Zhou, Journal of hazardous materials, 2011, 189, 150-157.
17 B. M. Reddy, A. Khan, Y. Yamada, T. Kobayashi, S. Loridant and J. C. Volta, Journal of Physical Chemistry B, 2003, 107, 11475-11484.
18 J. Kašpar, P. Fornasiero and M. Graziani, Catalysis Today, 1999, 50, 285-298.
19 G. Zhang, Z. Zhao, J. Xu, J. Zheng, J. Liu, G. Jiang, A. Duan and H. He, Applied Catalysis B: Environmental, 2011, 107, 302-315.
20 A. E. Nelson and K. H. Schulz, Applied Surface Science, 2003, 210, 206-221.
21 Q. Wang, G. Li, B. Zhao and R. Zhou, Applied Catalysis B: Environmental, 2010, 100, 516-528.
22 B. Zhao, C. Yang, Q. Wang, G. Li and R. Zhou, Journal of Alloys and Compounds, 2010, 494, 340-346.
23 A. Iglesias-Juez, Journal of Catalysis, 2004, 221, 148-161.
24 X. Yang, L. Yang, S. Lin and R. Zhou, The Journal of Physical Chemistry C, 2015, 119, 6065-6074.
25 R. C. R. Neto and M. Schmal, Applied Catalysis A: General, 2013, 450, 131-142.
26 X. Wu, X. Wu, Q. Liang, J. Fan, D. Weng, Z. Xie and S. Wei, Solid State Sciences, 2007, 9, 636-643.
27 J. Guo, D. Wu, L. Zhang, M. Gong, M. Zhao and Y. Chen, Journal of Alloys and Compounds, 2008, 460, 485-490.
28 A. Varez, E. Garcia-Gonzalez, J. Jolly and J. Sanz, Journal of the European Ceramic Society, 2007, 27, 3677-3682.
29 L. Li, F. Chen, J.-Q. Lu and M.-F. Luo, The Journal of Physical Chemistry A, 2011, 115, 7972-7977.
30 T. Taniguchi, T. Watanabe, N. Sugiyama, A. K. Subramani, H. Wagata, N. Matsushita and M. Yoshimura, The Journal of Physical Chemistry C, 2009, 113, 19789-19793.
31 A. Nakajima, A. Yoshihara and M. Ishigame, Physical Review B, 1994, 50, 13297-13307.
32 T. Hirata, Journal of Physics and Chemistry of Solids, 1995, 56, 951-957.
33 R. Si, Y.-W. Zhang, S.-J. Li, B.-X. Lin and C.-H. Yan, The Journal of Physical Chemistry B, 2004, 108, 12481-12488.
34 A. Baylet, S. Royer, P. Marécot, J. M. Tatibouët and D. Duprez, Applied Catalysis B: Environmental, 2008, 81, 88-96.
35 M. Li, Z. Feng, G. Xiong, P. Ying, Q. Xin and C. Li, The Journal of Physical Chemistry B, 2001, 105, 8107-8111.
36 G. Ranga Rao, P. Fornasiero, R. Di Monte, J. Kašpar, G. Vlaic, G. Balducci, S. Meriani, G. Gubitosa, A. Cremona and M. Graziani, Journal of Catalysis, 1996, 162, 1-9.
37 J. Zhou, K. Wu, W. Wang, Y. Han, Z. Xu, H. Wan, S. Zheng and D. Zhu, Applied Catalysis B: Environmental, 2015, 162, 85-92.
38 M. Yang, M. Shen, J. Wang, J. Wen, M. Zhao, J. Wang and W. Wang, The Journal of Physical Chemistry C, 2009, 113, 12778-12789.
39 B. Azambre, I. Atribak, A. Bueno-Lopez and A. Garcia-Garcia, Journal of Physical Chemistry C, 2010, 114, 13300-13312.
40 L. F. Bobadilla, O. Marie, P. Bazin and M. Daturi, Catalysis Today, 2013, 205, 24-33.
41 B. Azambre, L. Zenboury, A. Koch and J. V. Weber, Journal of Physical Chemistry C, 2009, 113, 13287-13299.
42 M. Konsolakis and I. V. Yentekakis, Topics in Catalysis, 2013, 56, 165-171.
43 A. Martínez-Arias, Journal of Catalysis, 2001, 204, 238-248.
44 V. Matsouka, M. Konsolakis, R. M. Lambert and I. V. Yentekakis, Applied Catalysis B-Environmental, 2008, 84, 715-722.